Nano Energy 51 (2018) 185–191

Contents lists available at ScienceDirect

Nano Energy

journal homepage: www.elsevier.com/locate/nanoen

Full paper

Highly-sensitive and highly-correlative flexible motion sensors based on asymmetric piezotronic effect

Jae Won Lee[a], Byeong Uk Ye[b], Zhong Lin Wang[c], Jong-Lam Lee[d], Jeong Min Baik[a,*]

[a] School of Materials Science and Engineering, KIST-UNIST-Ulsan Center for Convergent Materials, Ulsan National Institute of Science and Technology (UNIST), Ulsan 44919, Republic of Korea
[b] Max Planck Institute for Biophysical Chemistry, Institute for Physical Chemistry, Göttingen University, Göttingen 37077, Germany
[c] School of Material Science and Engineering, Georgia Institute of Technology, Atlanta, GA 30332-0245, United States
[d] Division of Advanced Materials Science, Department of Materials Science and Engineering, Pohang University of Science and Technology (POSTECH), Pohang, Gyungbuk 37673, Republic of Korea

ARTICLE INFO

Keywords:
Asymmetric polarization
Piezotronic effect
High-correlation
Nanogenerator
Motion sensor

ABSTRACT

This paper describes two highly-sensitive flexible motion sensors (piezoelectric nanogenerators and ultraviolet light emitting diodes based flexible GaN) based on asymmetric polarization created across flexible GaN film and very high correlations of the sensors for precise motion measurement. The operation mechanism is based on piezotronic effect using polarization charges at the interface for tuning the electronic and optoelectronic processes. The nanogenerator showed very high sensitivity (S = 93 at 0.45% under concave bending) and the convex bending led to the decrease of the sensitivity to 24. The electroluminescence intensity also almost linearly decreased with the change of the bending direction, clearly shown in the confocal scanning electroluminescence microscopy images with the bending motion. The two sets of measures showed very high correlations (R^2 = 0.98 and 0.96 under concave and convex bending, respectively) with very sensitive directional information. This approach makes to recognize the direction of bending as well as to measure the magnitude of the strain for realizing multi-functional, motion detection sensing devices.

1. Introduction

Exceptionally sensitive sensors that can accurately provide motion information from a human body such as the magnitude of strain and bending direction are becoming increasingly important to satisfy functional and structural demands for wearable devices and robotic devices [1–6]. Wearable motion sensing technologies such as human motion detection [7–9], electronic skins [10,11], and real-time healthcare monitoring [12–14], are considered as key components in the development of diagnostic and other electronic applications, associated with health care. As an innovative technology in the Fourth Industrial Revolution, the motion sensors with high sensitivity and multiple functions in robots fields are also essential for the purpose of measuring the bending of the joint and for surgical tools such as the catheter [15,16]. With the importance of the sensors, many sensors have been developed and successfully demonstrated in real applications such as soft robotics [17,18], human-machine interface systems [19,20], and smart suits for babies [21], athletes or soldiers [22,23]. Recently, self-powered strain sensors based on piezoelectric effects and triboelectric effects were developed, and high sensitivity was demonstrated without any external power [24–26].

In the existing methods, strains are detected in various ways, for example, by measuring the change in electrical resistance or capacitance with the applied strain [27], or by optically measuring the intensity of the reflected light that shifts in response to variations in strain [28,29]. Although these methods have been proven to be quite effective in real applications, it may not be easy to accurately identify the strained conditions applied to the sensors if only one method is used. Actually, the integration of two and more sensors to improve the accuracy was already applied to the commercial product, such as the detection of angle, in which the sensors were designed to complement each other [30]. To generate multiple types of information such as strain, pressure, bending direction etc., various sensing devices will be required to improve the reliability of the information. Therefore, it is essential to obtain multiple data sets from individual strain sensors and evaluating the correlation between the sets, to confirm the motion information, such as precise values of strain, as well as accurate bending direction.

Here, we demonstrate a facile strategy to provide accurate motion information that utilizes two methods based on the large piezoelectric

* Corresponding author.
E-mail address: jbaik@unist.ac.kr (J.M. Baik).

https://doi.org/10.1016/j.nanoen.2018.06.059
Received 22 April 2018; Received in revised form 5 June 2018; Accepted 17 June 2018
Available online 21 June 2018

effects of Gallium nitride (GaN) and asymmetric polarization created inside flexible GaN thin film. GaN has been considered to be a famous direct wide bandgap semiconductor in light-emitting diodes (LEDs) because of the excellent optoelectronic properties such as small exciton binding energy (~ 21 meV) and high electron mobility (~ 350 cm^2 V^{-1} s^{-1}) [31]. The theoretical piezoelectric constants were reported to be e_{15} = −0.49 C/m^2, e_{31} = −0.49 C/m^2, and e_{33} = 0.73 C/m^2, showing strong piezoelectric effects [32]. The electronic properties such as resistivity, carrier density and mobility can be well-controlled by the growth parameter tuning. It also offers a number of excellent properties such as good chemical stability, high mechanical robustness, and environmental compatibility, and thus, efficiently converting ambient mechanical energies into electricity [33]. Owing to the polarization of wurtzite structured GaN, a piezoelectric potential (piezopotential) is created in the crystal by applying a stress owing to the presence of one atomic-layer thick polarization charges at the surface/interface, which can significantly tune the electronic and photonic processes, and is thus referred to a piezotronic effect [34–36]. Based on these unique properties, two sets of measures were made, that is, the generated voltages of flexible GaN piezoelectric nanogenerator and the ultraviolet (UV) light intensities of the flexible GaN UV LEDs with bending motion, possible chosen for accurate motion information. The 2-in. wafer-scale laser lift-off (LLO) process was employed to fabricate the two flexible GaN devices. The spontaneous polarization created inside GaN also produced asymmetric Schottky barrier height (SBH) at the interface of metals and GaN, and affected the electron-hole recombination rate across the *p-n* junction, offering significant potential to develop high and directional sensing approaches. The nanogenerator showed very high sensitivity (S = 93 at 0.45%) under the concave bending, while it significantly decreased to 24 under the convex bending. The electroluminescence (EL) intensity of the LEDs almost linearly increased when device was bent from convex to concave bending motion, clearly shown by confocal scanning electroluminescence microscopy (CSEM) images. These results clearly show that the sensor can provide exact bending information. When we correlated the two sets of measures, very high correlations (R^2 = 0.98 and 0.96 under concave and convex bending, respectively) were obtained, showing the reliability of the strained conditions measured.

2. Experimental

2.1. Fabrication of flexible GaN piezoelectric nanogenerators

A 500-nm-thick undoped GaN buffer layer and 800-nm-thick *p*-type GaN layer were grown in sequence on *c*-plane sapphire substrates using metal-organic chemical vapor deposition (MOCVD). For the growth of GaN, trimethylgallium (TMG) and ammonia (NH_3) were used. The Mg concentration was controlled by varying the flow rate of bis-(cyclopentadienyl)-magnesium (Cp_2Mg) from 150 sccm to 1200 sccm while the growth temperature was fixed at 950 °C. The samples were annealed for the accepter activation. For the fabrication of flexible *p*-GaN thin films, Ti/Au (20/200 nm) electrodes were deposited on the *p*-type GaN, followed by annealing at 300 °C for 1 min in air ambient. And then, a copper (Cu) layer with a thickness of 20 μm was electroplated on the Ti/Au seeding layers, and subsequently the laser lift-off (LLO) process for separating the structures from the sapphire substrate was performed in air using a Lambda Physik Lextra 200 KrF pulsed excimer laser. The 248 nm wavelength of the KrF laser was used to irradiate the back side of the sapphire at an energy density of 254.2 mJ/cm^2. After the LLO, the undoped GaN layer was etched away by ICP etching, leaving *p*-type GaN layer. Ti/Au contact was then deposited on the *p*-type GaN as a top electrode. PET films were then attached at the bottom sides of the device, which act as the plastic substrates.

2.2. Fabrication of flexible GaN UV LEDs, by LLO process

For flexible GaN UV LEDs, a 500-nm-thick undoped GaN buffer layer, 2-μm-thick *n*-type GaN, and 800-nm-thick *p*-type GaN layer were grown in sequence on *c*-plane sapphire substrates using metal-organic chemical vapor deposition (MOCVD). The *n*-type GaN film was grown using SiH_4 for *n*-type doping and the Mg concentration was fixed by flowing the Cp_2Mg with 1200 sccm for *p*-type GaN film. Ni/Au (20/200 nm) electrodes were then deposited on the *p*-type GaN, followed by annealing at 300 °C for 1 min in air ambient, to decrease the Ohmic junction resistances. After the LLO process, the undoped GaN was etched away by ICP etching, leaving *n*-type and *p*-type GaN layer, followed by trench etching. Ti/Au (20/200 nm) was then deposited on the *p*-type GaN as a top electrode. PET for plastic substrates were then attached at the bottom sides of the device.

2.3. Characterization and measurements

The scanning electron microscopy (SEM) was done using a FEI Nanonova 230 with an accelerating voltage of 10 kV. The electrical properties of the GaN films were analyzed using Hall measurement systems (LakeShore, Model 7600). To detect currents and voltages generated by flexible *p*-type GaN film nanogenerator, a Keithley 6485 picoammeter and Keithley 2182 A voltammeter were used. To ensure regular and continuous electricity generation, bending testers (Z-tec) were used. The LED luminance (brightness) was then calculated from the known portion of the forward emission and the LED output spectra. Images of LED output were recorded with an Olympus MVX10 using a cooled charge coupled device (CCD) detector (iXon3 888). All measurements were performed under ambient conditions at room temperature.

3. Results and discussion

The schematic diagrams of the flexible GaN piezoelectric nanogenerators based on *p*-type GaN film fabrication processes are shown in Fig. 1a and detailed information is given in the Experimental section. Fig. 1b shows I-V curves of the device carried out at various staining conditions. Here, the hole concentration was measured to be approximately 6.55 × 10^{16} cm^{-3}. It is clearly seen that the device exhibits a typical behavior of the Schottky diode. Strain values in a thin film are calculated with tensile strain defined as positive and compressive strain defined as negative along the transverse direction, respectively. Thus, along the vertical direction, it is calculated that the compressive strain is applied during convex bending, while the tensile strain is applied during concave bending (see the “calculation of strain” section in the Supplementary Materials) [37–39]. When positive voltage was applied to the drain, the current through the device increased under the convex bending, while at concave bending, the current was decreased with the strain. Conversely, under negative drain bias, the opposite trend was observed with the current increasing with the concave bending and decreasing with the convex bending. Current values in device under various strains were measured at certain biases (2 V and −2 V) and plotted in Fig. 1c. It was clearly shown that the currents passing through the *p*-type GaN film almost linearly varied as the curvature of the surface changed from concave to convex. The characteristics of the I-V curves in Fig. 1b is the typical result of piezotronic effect, indicating that the carrier transport across the interface is modulated by piezopotential created by the applied strain [40–43].

The change in the current according to the straining conditions was investigated with the barrier height between the electrode and the *p*-type GaN film, by using the ultraviolet photoemission spectroscopy (UPS) spectrum. UPS measurements were performed to calculate the surface electronic properties such as the electron affinity and ionization energy of the films. Fig. 2a shows the onset of secondary electron peak and the valence band spectra of N- and Ga-face GaN films. The SBH in

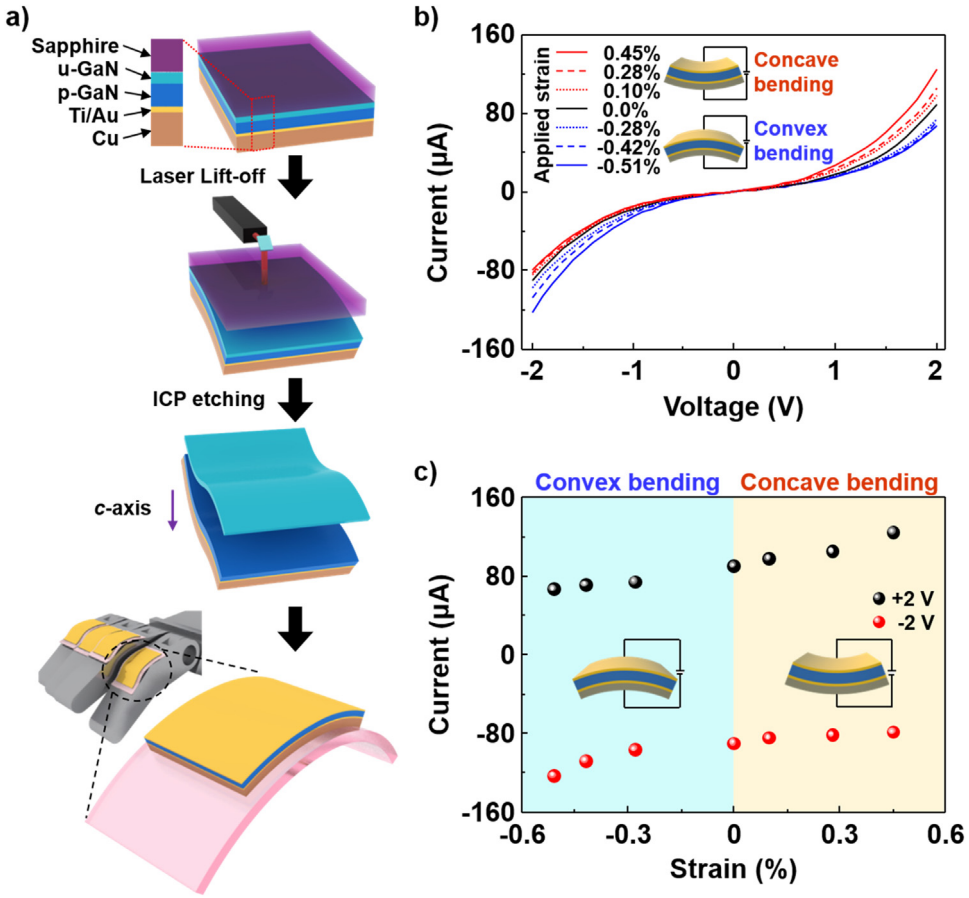

Fig. 1. (a) The schematic diagrams of the flexible *p*-type GaN nanogenerator fabrication process. (b) I-V curves carried out at various staining conditions. (c) Current values in a device under various strains measured at fixed biases (2 and − 2 V).

the metal/semiconductor interface is derived as the difference in the ionization potential (IP) for a *p*-type semiconductor and the metal work function by the Schottky-Mott model [44];

$$\phi_{Bp} = E_g - (\phi_m - \chi) = \mathrm{IP} - \phi_m \quad (1)$$

where ϕ_{Bp} is the SBH for *p*-type semiconductor and ϕ_m is the metal work function. The valence band spectra shifted toward lower binding energy by approximately 0.25 eV in the Ga-face sample, compared with the Ga-face sample. Assuming that the work function of *p*-type GaN is approximately 4.3 eV, it implies that the barrier height of the electrode is higher (∼ 0.25 eV) in N-face GaN than that in the Ga-face GaN, as shown in Fig. 2a.

Fig. 2b shows the change in the barrier height with various straining conditions, calculated from the currents measured in Fig. 1c. To calculate the changes of the SBH (ϕ_B), the following equation derived from the thermionic emission diffusion theory function [41];

$$\Delta\phi_B = \phi_{B\varepsilon} - \phi_{B0} = -\frac{KT}{q} \cdot \ln(I_\varepsilon / I_0) \quad (2)$$

where I_ε and I_0 are the currents measured at the devices with and without strained films when a certain voltage is applied, respectively. $\phi_{B\varepsilon}$ and ϕ_{B0} are the SBHs, respectively. The calculated values at − 2 V and 2 V are summarized in Fig. 2b. When the films were under convex bending at 2 V, the barrier height increased by 7.6 meV and decreased by 9.7 meV at concave bending. Thus, the change in barrier height of 17.3 meV was observed with the bending direction. This made the barrier height at the interface between the electrode and N-face GaN larger, but the barrier height at the interface between the electrode and Ga-face GaN smaller, thereby, the barrier height asymmetry increased, as shown in Fig. 2c. When − 2 V was applied, it shows a similar numerical value, but the barrier height decreased and then increased with the same bending direction. This decreased the barrier height asymmetry. The change in the SBH with various straining conditions can be understood in terms of the piezopotential by piezoelectric polarization and spontaneous polarization potentials. When the film is under concave bending, the orientation of the spontaneous and piezoelectric polarization is parallel along the *c*-axis, resulting in an increase in the total electrostatic potential. This will increase the negative charges induced at the interface of metal and N-face GaN, which attract the holes toward the interface, and thereby decrease the depleted region and the SBH; while the SBH will be increased at the interface of metal and Ga-face GaN by the positive charges to repel the electrons away from the interface, resulting in a further depleted interface [45–47]. In the case of the convex bending, the total potential is decreased by the different direction of both polarizations. This will increase the degree of the asymmetry of the SBHs at both interfaces, as expected from piezotronic effect.

By using the COMSOL Multiphysics, we calculated the total electric potential distribution along the *c*-axis in the *p*-type GaN film under convex and concave bending strain, by using a simple rectangular model composed of 500 nm-thick film under the load of 640 μN for strain of 0.45%, as shown in Fig. S1. The material parameters of the GaN are given as follows: transverse isotropy possesses five independent elastic constants, denoted by C_{11} = 390 GPa, C_{12} = 145 GPa, C_{13} = 106 GPa, C_{33} = 398 GPa, and C_{44} = 105 GPa. The piezoelectric constants are e_{15} = −0.49 C/m^2, e_{31} = −0.49 C/m^2, and e_{33} = 0.73 C/m^2; the dielectric constants are k_{11} = k_{12} = 9.28, k_{33} = 10.01; and the density = 6150 kg/m^3 [32]. The total electric potential can be calculated by summing the piezopotential and the spontaneous polarization potentials, depending on the bending

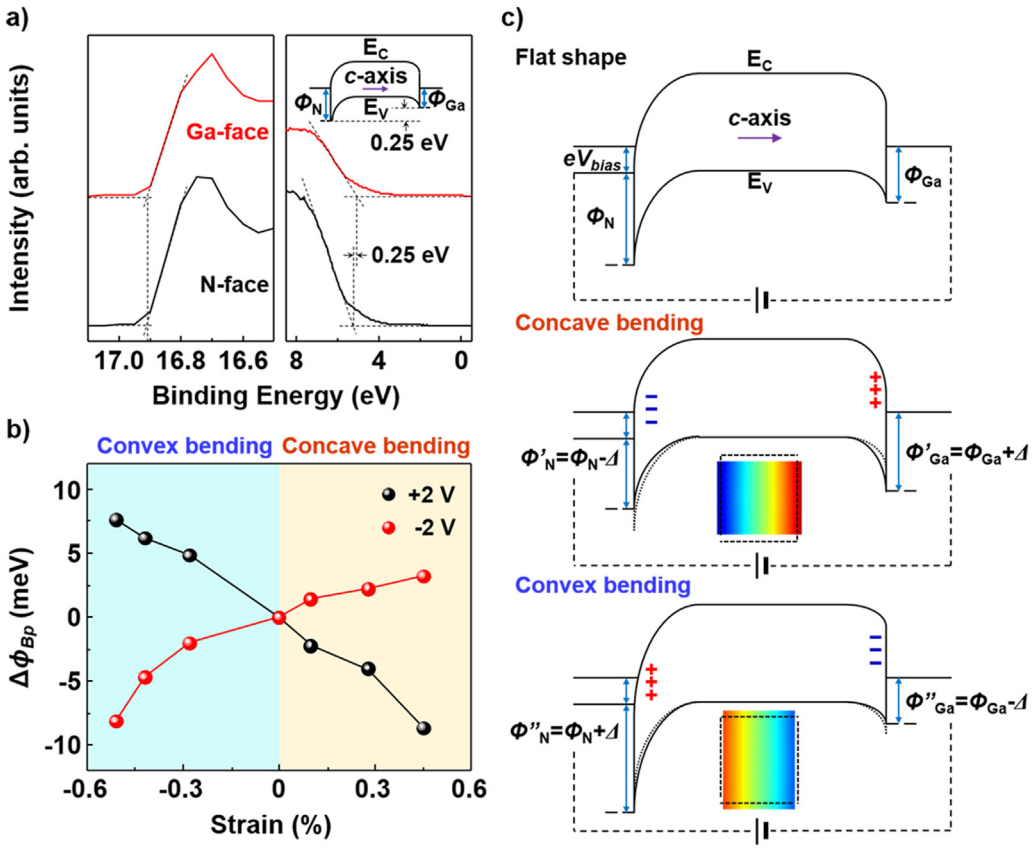

Fig. 2. (a) Valence band spectra and secondary electron cut-off of Ga-face and N-face sample. Energy band diagram under unbiased is shown in the inset. (b) The changes of the SBH (ϕ_B) with various straining conditions, calculated from the measured currents. (c) Energy band diagrams under unbending (flat shape), convex bending, and concave bending at applied voltage. red + and blue – mean positive piezoelectric polarization charges and negative piezoelectric polarization ch arges, respectively.

direction. When the film is under concave bending, as shown in Fig. S1a, a compressive stress is applied over the entire *p*-type GaN along the transverse direction (*a*-axis), resulting in the tensile strain to the film along the vertical direction (*c*-axis). If the compressive strain in the transverse direction under concave bending is defined as $\varepsilon = \Delta x/x$, the tensile strain (ε_z) in the vertical direction can be calculated to be $-0.18\varepsilon_x$ by using the Poisson ratio ($\nu = -\varepsilon_{vertical}/\varepsilon_{transverse} = -\varepsilon_z/\varepsilon_x = 0.18$) of the GaN material. On the other hand, the compressive strain is applied to the film along the vertical direction under convex bending, as shown in Fig. S1b.

Through bending of the flexible GaN piezoelectric nanogenerators, the instantaneous electrical outputs were measured, compared with the bending direction, as shown in the photos of Fig. 3a. The output voltages of the nanogenerators were measured by varying the bending direction under same condition with strains from 0.1% to 0.45%, as shown in Fig. 3b and c. When the film is under concave bending, the voltage increases from 0.18 V to 1.0 V with the strains, as shown in Fig. 3b; though when the film is under convex bending, the voltage is only generated from 0.05 V to 0.25 V, as shown in Fig. 3c. When the *p*-type GaN film was under convex bending, it generated an output voltage of approximately 1.0 V and an output current of 10.5 μA/cm^2 (see Fig. S2a). Here, the strain was measured to be approximately 0.45%. However, when the film was under concave bending, the output voltage of only 0.25 V was measured, that is, the output voltage was about 3.8 times higher at convex bending. This result was quite reproducible after several repeated experiments. These results may be understood by considering two factors. First, the total electrostatic potential under concave bending is larger than that under convex bending because the orientation of the spontaneous and piezoelectric polarization is parallel along the *c*-axis, thus, increasing the output voltage. Second, the carriers through the external circuits can be injected to the GaN film because of the decrease in the SBH at the interface between Ga-face and metal under convex bending [48–51]. This will decrease the output performance of the device.

In the flexible device composed of *n*-type GaN, there was no significant output, as shown in Fig. S2b. In *n*-type GaN, the electron concentration was measured to be approximately 1.06×10^{19} cm^{-3}, which was quite higher than the hole concentration in *p*-type GaN used so far. It was well-known that as the carrier concentration increased, the output voltage of the piezoelectric film decreased due to the piezopotential screening effects [52,53]. In general, the carrier concentration speeds up the rate at which the piezoelectric charges are screened and neutralized. Therefore, as the carrier concentration increases, the lifetime of the piezoelectric charges is reduced, resulting in small piezopotential and output performance. Here, we varied the Mg concentration from 0.7×10^{20} cm^{-3} to 5.7×10^{20} cm^{-3} when *p*-GaN film was grown, and the hole concentration and mobility were measured, as shown in Figs. S3 and S4. As the Mg concentration increases to 2×10^{20} cm^{-3}, the hole concentration increases. However, further increase of the Mg concentration decreases the hole concentration to 6.55×10^{16} cm^{-3}; almost similar as in previous reports [54]. The mobility decreases as the Mg concentration increases. When the output voltages were measured, they decreased as the hole concentration decreased under both bending conditions, as shown in Fig. S3. However, there was no relationship between the mobility and output voltage.

Finally, the strain can also be detected by measuring the intensity of the UV light emitted at the flexible devices composed of *p-n* junction, fabricated by LLO process and followed by the trenching etching, as shown in Fig. 4a. For the fabrication of the devices, as electrodes, Ti/Au (20/200 nm) and Ni/Au (20/200 nm) were deposited on *n*-type and *p*-type GaN, respectively, followed by annealing at 300 °C for 1 min in air ambient, to enhance the Ohmic contact. The EL intensities at various straining conditions under 2.5 V were measured, compared with the current changes obtained at the same voltage, as shown in Fig. 4b. The schematic and real measurement tool for measuring the EL intensities at various straining conditions are presented in Fig. S5. Both ends of the

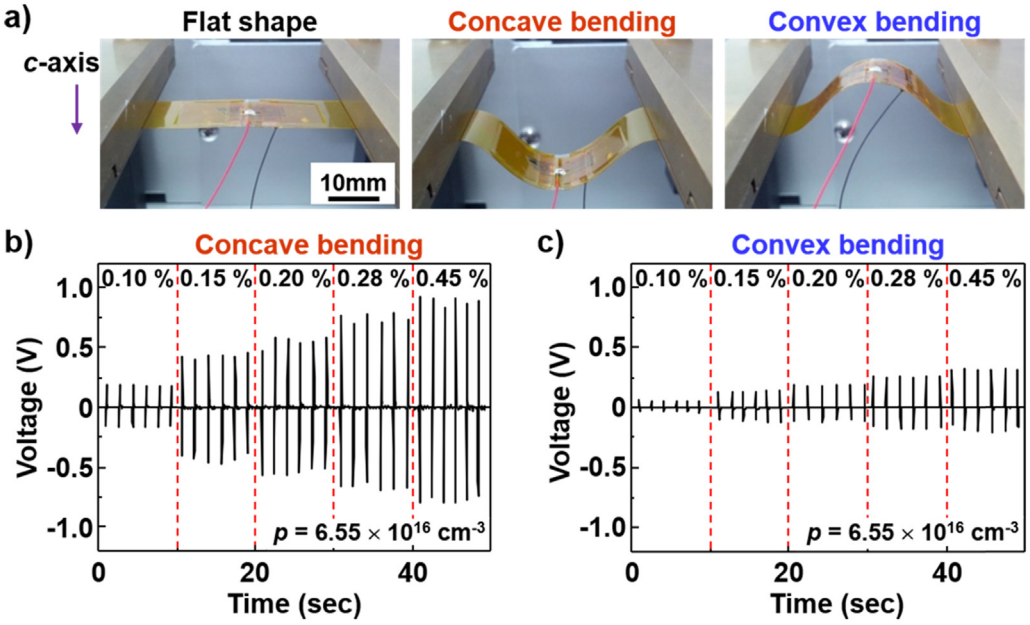

Fig. 3. (a) Photograph of the flexible GaN piezoelectric nanogenerator under unbending, concave bending, and convex bending. Output voltages of nanogenerator based on *p*-type GaN films with hole concentration of 6.55×10^{16} cm^{-3} under (b) concave and (c) convex bending with strains from 0.10% to 0.45%.

plastic substrates were fixed tightly on sample holders and a charge coupled device (CCD) detector could move up and down. To measure the intensities of the light at various straining conditions, focus lens equipped carefully were controlled the distance between the sample and the CCD detector of the tool. The intensities were also measured several times by tuning the distance and the highest intensities were plotted in Fig. 4b.

Under convex bending at the strain of 0.37%, the EL intensity decreased by 9.6%, compared to that under no bending. As the strain decreased and the device was under concave bending, the EL intensity almost linearly increased up to 8.2%. The CSEM images in Fig. 4c clearly demonstrates that the brightness increases under concave bending. Assuming that there is no potential generated inside the *n*-type GaN, based on the results of Fig. S2b, this result may be explained in terms of the electrostatic potential generated inside *p*-type GaN by the bending motion which changes the electron-hole recombination

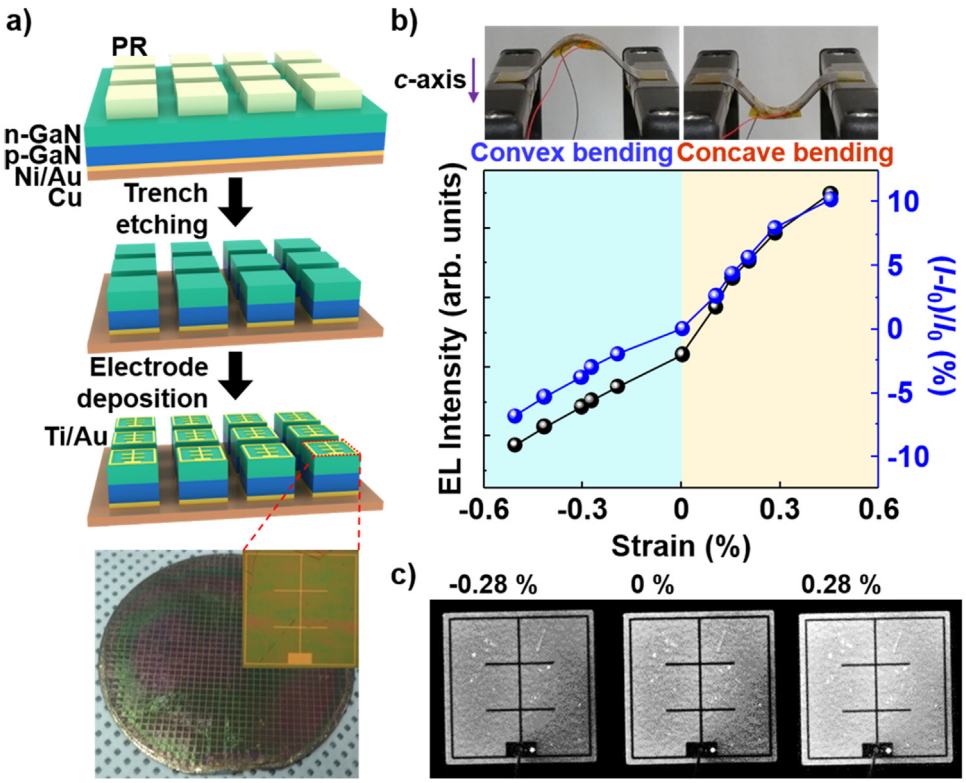

Fig. 4. (a) The schematic diagram of the flexible UV LEDs fabrication process. (b) The EL intensity and current changes under different straining conditions at 2.5 V. (c) confocal scanning electroluminescence microscopy (CSEM) images of the LEDs with applied strains at 2.5 V.

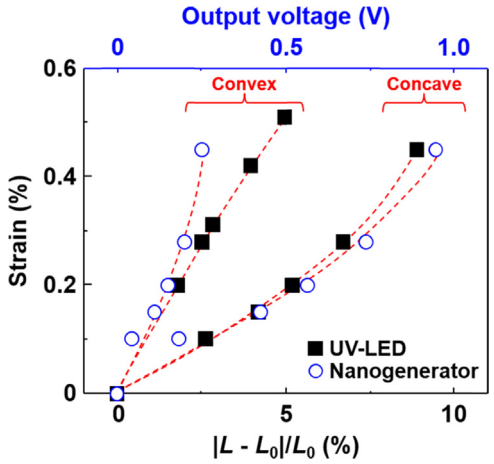

Fig. 5. The normalized EL intensities $(L\text{-}L_0)/L_0$ obtained by LEDs and output voltages generated by nanogenerator at various straining conditions. L_0 means the EL intensity of LED without any strain.

efficiency at the space charged region of the *p-n* junction. Fig. S6 is the schematic energy diagram illustrating the effect of piezopotential on modulating characteristics of the *p–n* junction. Under convex bending, the positive polarization charges repel the holes away from the interface in the *p*-type region, the conduction band edge at the p-type region shifts toward Fermi level, thereby, decreasing the electron–hole recombination rate. Concave bending induces tensile strain, promoting the accumulation of electrons and holes, thereby improving the efficiency of the UV-LED. It was also observed that the change of the EL intensity $\Delta L(\Delta L = L - L_0)$ measured with the bending motion was in good agreement with the current value. The strain sensitivity S can be defined as $S = (L - L_0)/L_0$, where L and L_0 denote the EL intensity with and without strain, respectively [24,55]. Here, in our instrument, L_0 is usually measured as approximately 2615. The sensitivity ($S = 0.09$ at 0.45%) of the film at the concave bending was substantially larger than that ($S = 0.05$ at 0.51%) at convex bending.

The strains at various straining conditions as recorded by both methods (i.e. output voltages and the EL intensities) were compared to evaluate the strain measurement accuracy, plotted in Fig. 5. At low strain (< 0.15%), the trends with the strains seem to be very similar, meaning that the strain can be detected exactly by using both methods as well as the bending information. As the strain increased, the sensitivity of the strain under concave bending became larger in *p*-type film than that in the *p-n* junction, while the sensitivity is smaller under convex bending. This indicates that the bending information is more apparent when the output voltages are used. This difference may be because the change in the barrier height with the strain is more sensitive than that in the depletion region inside the *p-n* junction. To identify the statistical relationship between output voltage of *p*-type film and the EL intensities curve of the *p-n* junction with various straining conditions, the coefficient of determination is resulted from set depending on bending direction (see the “calculation of correlation coefficient” section in the Supplementary Materials) [56]. The graph set showed excellent correlations ($R^2 = 0.98$ and 0.96 under concave and convex bending, respectively). Thus, by utilizing both methods, it is possible to accurately measure the direction of motion and the strain.

4. Conclusions

In summary, we reported a facile strategy to provide accurate motion information (i.e. the magnitude of strain and the direction of the bending motion) based on piezotronic effect using polarization charges at the interface for tuning the electronic and optoelectronic processes. The 2-in. wafer-scale laser lift-off process was employed to fabricate the flexible GaN piezoelectric nanogenerators and GaN LEDs, followed by the measurement of the generated voltages and light intensities with bending motion, respectively. The measured I-V curve fits well to the typical characteristics of piezotronic effect. The spontaneous polarization created inside flexible GaN made the SBH at the interface of metals and GaN asymmetric and affected the electron-hole recombination rate across the *p-n* junction, offering significant potential to develop high and directional sensing approaches. The nanogenerator showed very high sensitivity ($S = 93$ at 0.45%) under concave bending, while it significantly decreased to 24 under convex bending. The EL intensities of the flexible LEDs linearly increased as it was bent from convex to concave bending motion, clearly shown in the CSEM images with the bending motion. Thus, very sensitive directional sensing performance was successfully demonstrated. When we correlated the two sets of measures, very high correlations ($R^2 = 0.98$ and 0.96 under concave and convex bending, respectively) were obtained, showing the reliability of the strained conditions measured. This approach was expected to be an attractive potential strategy, providing the high possibility for realizing multi-functional, motion detection sensing devices.

Acknowledgements

This work was financially supported by the Pioneer Research Center Program through the National Research Foundation of Korea funded by the Ministry of Science, ICT, & Future Planning (NRF-2013M3C1A3063602), by the Institute for Information & communications Technology Promotion (IITP) grant funded by the Korea government (MSIP) (No. 2017000910001100, Development of multi-material 3D printing technologies for flexible motion detection and control sensor modules), and by the 2018 Research Fund (1.180061.01) of UNIST (Ulsan National Institute of Science & Technology).

Appendix B. Supporting information

Supplementary data associated with this article can be found in the online version at http://dx.doi.org/10.1016/j.nanoen.2018.06.059.

References

[1] T. Someya, Y. Kato, T. Sekitani, S. Iba, Y. Noguchi, Y. Murase, H. Kawaguchi, T. Sakurai, Proc. Natl. Acad. Sci. USA 102 (2005) 12321–12325.
[2] T. Someya, T. Sekitani, S. Iba, Y. Kato, H. Kawaguchi, T. Sakurai, Proc. Natl. Acad. Sci. USA 101 (2004) 9966–9970.
[3] X. Xiao, L.Y. Yuan, J.W. Zhong, T.P. Ding, Y. Liu, Z.X. Cai, Y.G. Rong, H.W. Han, J. Zhou, Z.L. Wang, Adv. Mater. 23 (2011) 5440–5444.
[4] T.Q. Trung, N.T. Tien, D. Kim, M. Jang, O.J. Yoon, N.-E. Lee, Adv. Funct. Mater. 24 (2014) 117–124.
[5] Y. Cheng, R. Wang, J. Sun, L. Gao, Adv. Mater. 27 (2015) 7365–7371.
[6] C. Pang, C. Lee, K.-Y. Suh, J. Appl. Polym. Sci. 130 (2013) 1429–1441.
[7] T. Yamada, Y. Hayamizu, Y. Yamamoto, Y. Yomogida, A. Izadi-Najafabadi, D.N. Futaba, K. Hata, Nat. Nanotechnol. 6 (2011) 296–301.
[8] C.S. Boland, U. Khan, C. Backes, A. O'Neill, J. McCauley, S. Duane, R. Shanker, Y. Liu, I. Jurewicz, A.B. Dalton, J.N. Coleman, ACS Nano 8 (2014) 8819–8830.
[9] Q. Liu, J. Chen, Y. Li, G. Shi, ACS Nano 10 (2016) 7901–7906.
[10] N. Lu, C. Lu, S. Yang, J.A. Rogers, Adv. Funct. Mater. 22 (2012) 4044–4050.
[11] T. Yang, W. Wang, H. Zhang, X. Li, J. Shi, Y. He, Q.S. Zheng, Z. Li, H. Zhu, ACS Nano 9 (2015) 10867–10875.
[12] Y. Wang, L. Wang, T. Yang, X. Li, X. Zang, M. Zhu, K. Wang, D. Wu, H. Zhu, Adv. Funct. Mater. 24 (2014) 4666–4670.
[13] X. Wang, Y. Gu, Z. Xiong, Z. Cui, T. Zhang, Adv. Mater. 26 (2014) 1336–1342.
[14] S. Ryu, P. Lee, J.B. Chou, R. Xu, R. Zhao, A.J. Hart, S.G. Kim, ACS Nano 9 (2015) 5929–5936.
[15] D.-H. Kim, N. Lu, R. Ma, Y.-S. Kim, R.-H. Kim, S. Wang, J. Wu, S.M. Won, H. Tao, A. Islam, K.J. Yu, T.-I. Kim, R. Chowdhury, M. Ying, L. Xu, M. Li, H.-J. Chung, H. Keum, M. McCormick, P. Liu, Y.-W. Zhang, F.G. Omenetto, Y. Huang, T. Coleman, J.A. Rogers, Science 333 (2011) 838–843.
[16] G. Shi, Z.H. Zhao, J.H. Pai, I. Lee, L.Q. Zhang, C. Stevenson, K. Ishara, R.J. Zhang, H.W. Zhu, J. Ma, Adv. Funct. Mater. 26 (2016) 7614–7625.
[17] J.C. Yeo, H.K. Yap, W. Xi, Z. Wang, C.-H. Yeow, C.T. Lim, Adv. Mater. Technol. 1 (2016) 1600018.
[18] H.K. Yap, H.Y. Ng, C.-H. Yeow, Soft Robot. 3 (2016) 144–158.
[19] S. Lim, D. Son, J. Kim, Y.B. Lee, J.K. Song, S. Choi, D.J. Lee, J.H. Kim, M. Lee, T. Hyeon, D.H. Kim, Adv. Funct. Mater. 25 (2015) 375–383.
[20] E. Roh, B.-U. Hwang, D. Kim, B.-Y. Kim, N.-E. Lee, ACS Nano 9 (2015) 6252–6261.
[21] M. Catrysse, R. Puers, C. Hertleer, L. Van Langenhove, H. van Egmond, D. Matthys,

Sens. Actuators, A 114 (2004) 302–311.
[22] S.L.P. Tang, Trans Inst, Meas. Control 29 (2007) 283–300.
[23] Q. Li, L.-N. Zhang, X.-M. Tao, X. Ding, Adv. Healthc. Mater. 6 (2017) 1601371.
[24] J. Chun, N.-R. Kang, J.-Y. Kim, M.-S. Noh, C.-Y. Kang, D. Choi, S.-W. Kim, Z.L. Wang, J.M. Baik, Nano Energy 11 (2015) 1–10.
[25] J. Zhong, Q. Zhong, Q. Hu, N. Wu, W. Li, B. Wang, B. Hu, J. Zhou, Adv. Funct. Mater. 25 (2015) 1798–1803.
[26] R. Yu, C. Pan, J. Chen, G. Zhu, Z.L. Wang, Adv. Funct. Mater. 23 (2013) 5868–5874.
[27] M. Amjadi, A. Pichitpajongkit, S. Lee, S. Ryu, I. Park, ACS Nano 8 (2014) 5154–5163.
[28] A.D. Kersey, M.A. Davis, H.J. Patrick, M. LeBlanc, K.P. Koo, C.G. Askins, M.A. Putnam, E.J. Friebele, J. Light. Technol. 15 (1997) 1442–1463.
[29] B.M. Quandt, L.J. Scherer, L.F. Boesel, M. Wolf, G.-L. Bona, R.M. Rossi, Adv. Healthc. Mater. 4 (2015) 330–355.
[30] H.J. Luinge, P.H. Veltink, Med. Biol. Eng. Comput. 43 (2005) 273–282.
[31] W. Shan, B.D. Little, A.J. Fischer, J.J. Song, B. Goldenberg, W.G. Perry, M.D. Bremser, R.F. Davis, Phys. Rev. B 54 (1996) (16 369-16 372).
[32] C.T. Huang, J.H. Song, W.F. Lee, Y. Ding, Z.Y. Gao, Y. Hao, L.J. Chen, Z.L. Wang, J. Am. Chem. Soc. 132 (2010) 4766–4771.
[33] M. Rais-Zadeh, V. Gokhale, A. Ansari, M. Faucher, D. Theron, Y. Cordier, L. Buchaillot, J. Microelectromech. Syst. 23 (2014) 1252–1271.
[34] W. Wu, X. Wen, Z.L. Wang, Science 340 (2013) 952–957.
[35] C. Pan, L. Dong, G. Zhu, S. Niu, R. Yu, Q. Yang, Y. Liu, Z.L. Wang, Nat. Photonics 7 (2013) 752–758.
[36] W. Wu, Z.L. Wang, Nat. Rev. Mater. 1 (2016) 16031.
[37] R. Yang, Y. Qin, L. Dai, Z.L. Wang, Nat. Nanotechnol. 4 (2009) 34–39.
[38] K.-I. Park, S. Xu, Y. Liu, G.-T. Hwang, S.-J.L. Kang, Z.L. Wang, K.J. Lee, Nano Lett. 10 (2010) 4939–4943.
[39] J.-H. Lee, K.Y. Lee, B. Kumar, N.T. Tien, N.-E. Lee, S.-W. Kim, Energy Environ. Sci. 6 (2013) 169–175.
[40] J. Zhou, P. Fei, Y.D. Gu, W.J. Mai, Y.F. Gao, R. Yang, G. Bao, Z.L. Wang, Nano Lett. 8 (2008) 3973–3977.
[41] J. Zhou, Y.D. Gu, P. Fei, W.J. Mai, Y.F. Gao, R.S. Yang, G. Bao, Z.L. Wang, Nano Lett. 8 (2008) 3035–3040.
[42] J. Zhou, P. Fei, Y. Gao, Y. Gu, J. Liu, G. Bao, Z.L. Wang, Nano Lett. 8 (2008) 2725–2730.
[43] X. Wang, R. Yu, C. Jiang, W. Hu, W. Wu, Y. Ding, S. Li, Z.L. Wang, Adv. Mater. 28 (2016) 7234–7242.
[44] S.M. Sze, K.K. Ng, Physics of Semiconductor Devices, Wiley, Hoboken, NJ, USA, 2007.
[45] Z.L. Wang, Adv. Mater. 24 (2012) 4632–4646.
[46] W. Wu, C. Pan, Y. Zhang, X. Wen, Z.L. Wang, Nano Today 8 (2013) 619–642.
[47] J. Shi, M.B. Starr, X.D. Wang, Adv. Mater. 24 (2012) 4683–4691.
[48] C.Y. Chen, G. Zhu, Y.F. Hu, J.W. Yu, J.H. Song, K.Y. Cheng, L.H. Peng, L.J. Chou, Z.L. Wang, ACS Nano 6 (2012) 5687–5692.
[49] V.A. Fonoberov, A.A. Balandin, J. Appl. Phys. 94 (2003) 7178–7186.
[50] Z. Zhao, X. Pu, C. Han, C. Du, L. Li, C. Jiang, W. Hu, Z.L. Wang, ACS Nano 9 (2015) 8578–8583.
[51] S. Lu, Q. Liao, J. Qi, S. Liu, Y. Liu, Q. Liang, G. Zhang, Y. Zhang, Nano Res. 9 (2016) 372–379.
[52] J.I. Sohn, S.N. Cha, B.G. Song, S. Lee, S.M. Kim, J. Ku, H.J. Kim, Y.J. Park, B.L. Choi, Z.L. Wang, J.M. Kim, K. Kim, Energy Environ. Sci. 6 (2013) 97–104.
[53] C.-H. Wang, W.-S. Liao, Z.-H. Lin, N.-J. Ku, Y.-C. Li, Y.-C. Chen, Z.-L. Wang, C.-P. Liu, Adv. Energy Mater. 4 (2014) 1400392.
[54] L.T. Romano, M. Kneissl, J.E. Northrup, C.G. Van De Walle, D.W. Treat, Appl. Phys. Lett. 79 (2001) 2734–2736.
[55] S. Gong, W. Schwalb, Y. Wang, Y. Chen, Y. Tang, J. Si, B. Shirinzadeh, W. Cheng, Nat. Commun. 5 (2014) 3132–3139.
[56] S.A. El-Safty, M.A. Shenashen, M. Ismael, M. Khairy, Adv. Funct. Mater. 22 (2012) 3013–3021.

Jae Won Lee is a Ph.D. candidate under the supervision of Prof. Jeong Min Baik at School of Materials Science and Engineering, Ulsan National Institute of Science and Technology (UNIST). His doctoral research focuses on development of composite and interlayer design based triboelectric generators for sustainable energy conversions, high output performance device, and fundamental study.

Dr. Byeong Uk Ye received his Ph.D. from Ulsan National Institute of Science and Technology (UNIST) in School of Materials Science and Engineering in 2017. Now he is currently working as a post-doctor fellow in Max Planck Institute for Biophysical Chemistry from 2017. His research interests are charge-enhancing mechanism with light-matter interaction in nano-phototronic devices for energy applications.

Dr. Zhong Lin Wang received his Ph.D. from Arizona State University in physics. He now is the Hightower Chair in Materials Science and Engineering, Regents' Professor, Engineering Distinguished Professor and Director, Center for Nanostructure Characterization, at Georgia Tech. His research on self-powered nanosystems has inspired the worldwide effort in academia and industry for studying energy for micro-nano-systems, which is now a distinct disciplinary in energy research and future sensor networks. He coined and pioneered the field of piezotronics and piezo-phototronics by introducing piezoelectric potential gated charge transport process in fabricating new electronic and optoelectronic devices.

Dr. Jong-Lam Lee is Professor in Department of Materials Science and Engineering, Pohang University of Science and Technology (POSTECH). He received his Ph.D. from Korea Advanced Institute of Science and Technology (KAIST) in Department of Materials Science and Engineering in 1985. His research interests include the fabrication of nanostructure and thin films, and the application of those materials to various devices including organic light-emitting diodes, solar cells, electrochemical reduction of carbon dioxide, and nanophotonics. Prof. Jong-Lam Lee is presently Namgo Chair Professor in the POSTECH.

Dr. Jeong Min Baik is Associate Professor in School of Materials Science and Engineering, Ulsan National Institute of Science and Technology (UNIST). He received his Ph.D. from Pohang University in Department of Materials Science and Engineering in 2006. His recent research interest is focused on the synthesis of nanomaterials and nanostructures such as nanoparticles, nanowires, nanolayers, and nanopores for the applications of Energy-Conversion Devices and Nano-photonic Devices. Particular interests are concerned with the development of Piezoelectric/Triboelectric Nanogenerators and Artificial Photosynthesis.